American Society of Mechanical Engineers

ASME Accepted Manuscript Repository

Institutional Repository Cover Sheet

Cranfield Collection of E-Research - CERES

ASME Paper Title: Co-firing of hydrogen and natural gas in a practical DLN combustor model

Authors: Rang Zhao, Uyioghosa Igie, David Abbott, Raditya Yudha Wiranegara

ASME Conf Title: ASME Turbo Expo 2023: Turbomachinery Technical Conference and Exposition

Volume/Issue: Volume 3B; Paper GT2023-103212 Date of Publication (VOR* Online) 28 September 2023

ASME Digital Collection URL: https://asmedigitalcollection.asme.org/GT/proceedings/GT2023/86960/V03BT04A031/1167902

DOI: https://doi.org/10.1115/GT2023-103212

*VOR (version of record)

Proceedings of ASME Turbo Expo 2023
Turbomachinery Technical Conference and Exposition
GT2023
June 26-30, 2023, Boston, Massachusetts, USA

GT2023-103212

Co-Firing of Hydrogen and Natural Gas in a Practical DLN Combustor Model

Rang Zhao Uyioghosa Igie David Abbott Raditya Yudha Wiranegara
Centre for Propulsion and Thermal Power Engineering,
Cranfield University
Cranfield, Bedfordshire, MK43 0AL, UK

ABSTRACT

To reduce carbon dioxide emissions, the combustion of natural gas-hydrogen blends in a lean premix gas turbine combustor has been investigated. Previous studies have mostly investigated the fuel blends at relatively low pressure (up to 5 bar) with relatively low hydrogen concentrations (up to 50vol%) on lab-scale or generic burner configurations. However, the influence of higher pressure and higher hydrogen content (over 50vol%) has not been widely studied, particularly on a practical industry-scale lean premixed burner as presented in this study. Such an operation is more challenging as it increases the turbulent flame speed gradient, which is an important factor in determining the likelihood of boundary layer flashback. A preliminary RANS-based Computational Fluid Dynamics (CFD) study has been conducted using ANSYS Fluent 2021R1, employing the Realizable K-Epsilon turbulence model and the Flamelet-Generated Manifold (FGM) combustion model. The combustor consists of a diffusion pilot and premixed main fuel nozzles. Methane-hydrogen blends of up to 90vol% hydrogen were investigated at a fixed fuel energy input. 100vol% methane at 15 bar pressure was taken as the baseline reference case. To investigate the flame characteristics, contour plots of OH mass fraction, equivalence ratios and temperatures (at different planes) are presented.

This study shows that the expected reduction in the flame length with increasing hydrogen concentration occurs up to 40vol%. Significantly different flame shapes (as indicated by OH contours) were seen at higher hydrogen content. For this model, the flashback occurred at 90vol% H_2 as indicated by a premature development of the flame within the nozzle of the main fuel burner. NO_x emissions are shown to progressively rise with increasing hydrogen content up to 60vol% but reduce as the hydrogen content increases to 70vol%. The decrease appears to be related to an improvement in the quality of fuel-air mixing. It is important to note that the apparent rate of increase in NOx with increasing hydrogen is dependent on the reporting approach used. When reporting conventionally (parts per million by volume corrected to 15% O_2 on a dry basis) the increase is significantly greater than when reporting on a mass per fuel energy input basis (gram per Joule). Reporting in the conventional manner disadvantages hydrogen because of the impact of oxygen consumption and water production on the corrections.

Keywords: hydrogen, natural gas, flashback, partially premixed, pilot

NOMENCLATURE

c	Reaction progress variable
CRZ	Centre recirculation zone
c_p	Specific heat capacity
FGM	Flamelet generated manifold
g_c	Turbulent flame speed gradient
g_f	Flow speed gradient
kth	kth species
LHV	Lower heating value
P_{th}	Fuel energy input
Xc	Scalar dissipation rate
λ	Thermal conductivity
$\dot{\omega}_k$	Kth species reaction rate
Φ	Equivalence ratio

1. INTRODUCTION

Gas turbines play an important role in power generation, providing baseload power, on-demand backup power and synchronous inertia for grid stability. This is likely to continue through the transition to a net zero-carbon future. Currently, the majority of gas turbine power generation is fueled by natural gas that produces carbon dioxide emissions. To reduce this, hydrogen is considered a potential clean fuel for gas turbines. However, hydrogen has significantly different combustion properties and behaviour compared to natural gas. In particular, has a higher flame speed than natural gas, hence increasing the flashback risk [1]. Burning natural gas-hydrogen blends or pure hydrogen in existing dry low NOx gas turbine combustors is challenging at higher hydrogen concentrations.

Investigations into the firing of blends of hydrogen and methane (the major constituent of natural gas) have been previously studied. Chterev and Boxx [2] measured the OH*-chemiluminescence of a technically-premixed hydrogen-natural

gas flame at 5 bar for up to 50vol%H_2. The study showed that the reaction rate and flame speed were enhanced by hydrogen addition, resulting in a shorter flame and higher flashback propensity. Griebel et al. [3] studied a hydrogen-methane air-premixed jet flame at 5 bar. As the hydrogen concentration increased, the lean blow-off critical equivalence ratio was shifted to the leaner side, indicating an increase in the reactivity, as the study showed. Whilst these studies were performed under relatively low pressure conditions, the influence of high pressure on the flame behaviour cannot be neglected. Sakhrieh et al. [4] showed that as the pressure was increased, the laminar flame speed of methane flame decreased. Additionally, Brower et al. [5] showed that the ignition delay time of a hydrogen-methane flame was affected by a variation in both pressure and hydrogen content. Ebi et al. [6] experimentally studied the impact of operating pressure on the boundary layer flashback propensity in hydrogen-methane swirl-stabilized turbulent flame. The study showed that the critical equivalence ratio Φ, at which the boundary layer flashback occurred, was shifted to the leaner side as the pressure increased, indicating an increase in flashback propensity due to high pressure. The impact of pressure on flashback propensity was explained by Lin et al. [7] using two parameters: flame speed gradient (g_c) and flow velocity gradient (g_f). The former represents the ability of the flame to resist the shear force and survive within the thin flow layer without extinguishing, whilst the latter represents the magnitude of the flow shear stress within the thin boundary layer. Flashback would occur if g_c is larger than g_f. The authors studied these parameters in a 85%H_2/15%N_2 flame and discovered that the critical equivalence ratio Φ was shifted from 0.47 to 0.38 when the pressure increased from 2.5 bar to 10 bar, indicating an increased probability of the flashback. To mitigate such a risk, the authors suggested decreasing the combustor inlet temperature, which generally requires cooling of compressor exit temperature.

A hydrogen-methane mixture fueled laboratory-scale hybrid burner with a separate pilot nozzle was studied by Fiolitakis et al.[8]. The study conducted experimental and numerical works at 13.7 bar with up to 50vol% hydrogen. In addition, the study included a variation in the pilot-to-total fuel ratio from 5% to 10%. As the pilot fuel ratio was increased, the study observed an increase in the pilot maximum flame temperature. Consequently, a higher thermal NO_X results from the correlation with flame temperature [9]. The study also showed that the flame length decreased, as the hydrogen share was increased [8]. In addition to these laboratory-scale burners studies, gas turbine engine manufacturers, such as Mitsubishi [10]-[11], Siemens [12]-[15], Ansaldo Energia [16]-[17] and GE [10][18] have successfully tested the co-firing of hydrogen-natural gas with various combustion technologies, as shown in **Figure 1**. It can be observed that typical Dry Low NO_x (DLN) burners can accommodate up to 30vol% hydrogen without significant modification in the burner configuration. Siemens SGT-800 can burn up to 80vol% hydrogen using the DLN approach. To burn medium hydrogen concentrations around 30vol% to 80vol% hydrogen, some technologies, such as micro-premix, sequential combustion and multi-cluster premix, have performed well in minimizing flame scale to control NO_x emissions. These methods can also facilitate fuel concentration scheduling close to the burner to avoid flashback.

To burn hydrogen without a flashback, diffusion combustion with steam or water injection to control NOx (i.e., Wet Low Emissions - WLE) is the current state-of-the-art for commercially available gas turbines. Progress in increasing the hydrogen capability of existing engines without water of stream injection is promising, yet there is still limited analysis of hydrogen-enriched natural gas flame in practical gas turbine combustors available in the open literature. The present study specifically addresses such a gap by adopting a Mitsubishi technology-inspired combustor developed and validated, as introduced in our earlier work [19] for 100vol% methane. The behaviour of hydrogen-methane blends from 0 to 90vol% hydrogen content at high pressure in a pilot-stabilized flame at a gas turbine scale was explored in the study. Such a configuration is not represented by the laboratory-scale experimental generic burners typically represented in the literature: such as the well-known PRECCINSTA technically-premixed swirl burner[2][20], the PSI swirl burner presented in Ebi et al. [6] and the Cardiff University HPGSB-2 generic swirl burner presented in Runyon et al. [21].

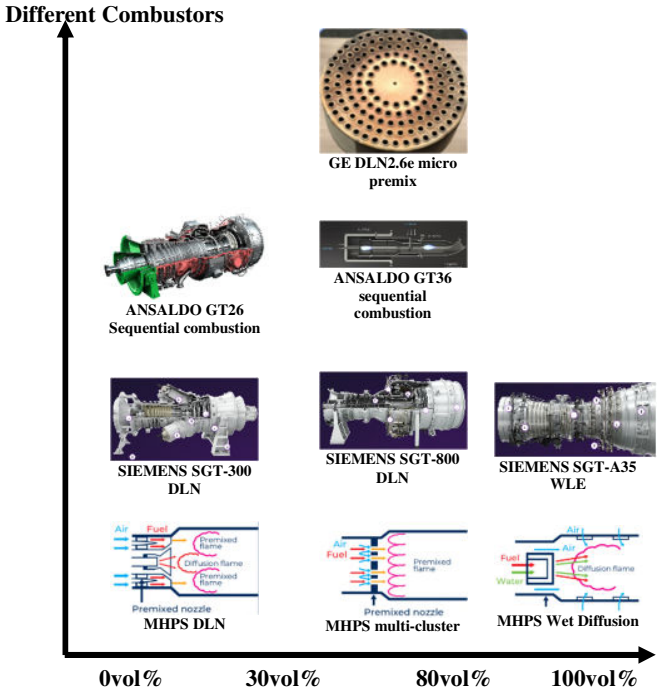

Figure 1. Current hydrogen capabilities in practical gas turbines[10]-[18]

2. BURNER UNDER INVESTIGATION AND METHODOLOGY

Wiranegara et al. [19] developed a combustor geometry and CFD model inspired by the M501G1 gas turbine [22]. The study presented here is to evaluate the impact of hydrogen addition on

the combustor originally designed for pure natural gas application. Furthermore, the study identified the changes in combustion performance as hydrogen concentration increases.

One-quarter section of the burner has been considered in the study, as depicted in **Figure 2.** It consists of two main premix nozzles and a pilot diffusion nozzle located at the centre. The one-quarter section of the burner has been considered mainly due to the significant computational cost of modelling the whole can. Two main nozzles, rather than a single main nozzle, are included to study the interactions between two neighbouring main nozzles. As shown in the figure, the main nozzles and pilot injectors are located at different circumferential locations, therefore two planes are created. These are the main mid-plane and the pilot mid-plane. These have been marked accordingly in **Figure 2a**. The pilot diffusion flame in the central recirculation zone (CRZ) generates some heat and reactive species to stabilize the main flame. At low load conditions, more pilot fuel is required to stabilize the flame. However, in this work, only the full-load condition was considered, given that the pressures are greater and hence more challenging for hydrogen-methane combustion as previously explained. The mass ratio of pilot/total fuel was fixed at 8%. The model also included some film cooling slots located at the chamber wall. The cooling slots introduce 9% of overall combustor air to protect the chamber wall from hot burnt gas.

The 90-degree section consists of two assumed periodic boundary surfaces. However, it should be noted that in the real combustor, the periodicity is not necessarily 90 degrees; it is unlikely in an engine configuration that the air supply to the burner will be truly symmetric. This assumption of 90-degree periodicity is a compromise of computational cost and accuracy.

Wiranegara et al. [19] generated the mesh using ICEM-CFD. A combination of tetrahedral and hexahedral meshes was used due to the complexity of the geometry in parts. The former was used for the burner and parts of the transition piece, while the latter was used mostly for the chamber, wall prisms and the remaining parts of the transition piece.

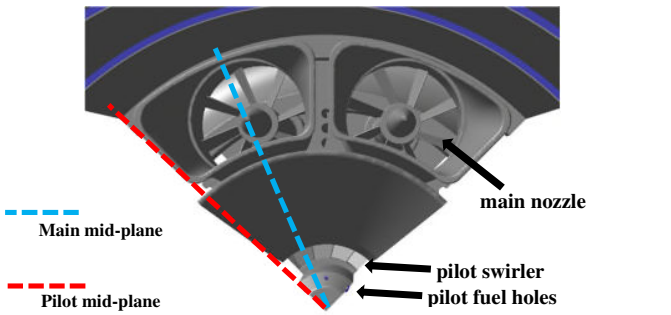

(a) Axial view of burner exit

(b) Side view of the burner

Figure 2. Schematic of one-quarter section of the burner

Figure 3 shows the side view of the meshed computational domain. For the mesh independency study, Wiranegara et al. [19] considered three grid cases; these are 6.3, 10.6 and 23.1 million nodes. The standard wall function was employed with a y+ of around 30 near the wall. For the mesh independency study, the boundary layer was kept the same for all the cases, to ensure that the investigation was only influenced by grid resolution. Also, the 10.6 million node case was identified to be a good compromise for accuracy and computational cost.

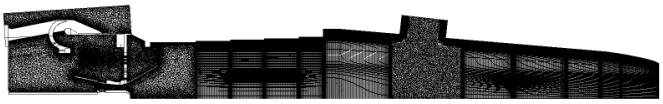

Figure 3. Side view of combustor model with mesh [19]

A commercial CFD software ANSYS Fluent 2021R1 was used for the CFD modelling, with the SIMPLE pressure-velocity coupling scheme. Also, the Realizable K-Epsilon (RKE) turbulence model was selected due to its good performance at simulating swirling flow [19][23]-[24]. GRI-3.0 [25] was adopted as the chemical kinetic mechanism and is typically more suitable for low hydrogen blends (<50vol%). For higher hydrogen blends, San Diego and O'Conaire are generally suggested [1]. Donohoe et al. [26] indicated that another kinetic mechanism, AramcoMech 1.3 [27] performs better than GRI-3.0 in predicting CH_4/H_2 combustion as the GRI-3.0 tends to underestimate the reactivity of hydrogen and overestimates the reactivity of hydrocarbon. Nevertheless, it was not appropriate to use different kinetic chemistry mechanisms at different hydrogen contents. This is to avoid the uncertainty of whether the predicted differences were due to real changes or inconsistencies in the mechanism used. Thus, this preliminary RANS study adopted only the GRI-3.0. This provides a consistent basis, also for the validated pure CH_4 baseline shown subsequently. From the known inaccuracies of the GRI-3.0 at increasing high hydrogen contents, qualitative trends will give useful insights into the likely behaviour of this combustor.

To model the flame, the Flamelet-generated manifold (FGM) combustion model was used. Shrivastava et al. [28] evaluated the performance of FGM in predicting several hydrogen-enhanced flames (jet flame, bluff body stabilized flame and micro-mix flame), and showed that FGM gave a reasonable agreement with experimental results. Zghal et al.[29] evaluated the performance of FGM in predicting a micromix burner with pure hydrogen and showed that FGM can produce a reasonable result with a low computational cost. This popular combustion model regards the 3-D flame as an ensemble of several 1-D laminar flames, where the internal flame structure is not significantly impacted by turbulence[30]-[31]. FGM can evaluate 1-D flamelet based on 1-D premixed flame or 1-D diffusion approach.

FGM can evaluate 1-D flamelet based on 1-D premixed flame or 1-D diffusion approach. In this study, the 1-D premixed flamelet type is selected as 92% of overall fuel is premixed in the main nozzles, thus the major flame characteristic is the premixed flame. In addition, FGM features preprocessing the flamelet

chemistry as a function of mean mixture fraction *f* and progress variable *c* [32]-[33]. FGM also integrates the turbulence-chemistry interaction into a Probability Density Function (PDF) table as a function of mean scalar and scalar variance [33]. These strategies make FGM relatively computationally inexpensive. To evaluate how many products have been created, the progress variable *c* is defined as a normalized product species mass fraction [30][34]:

$$\boldsymbol{c = \frac{\sum_{k=1}^{k=n} \alpha_k (Y_k - Y_k^u)}{\sum_{k=1}^{k=n} \alpha_k (Y_k^{eq} - Y_k^u)} = \frac{Y_c}{Y_c^{eq}}} \quad (1)$$

Where *k* denotes species index, *n* is the total number of species, α_k is 0 or 1 respectively for reactants species and several product species (generally CO_2, CO for hydrocarbon-contained fuel and H_2O for pure hydrogen), depending on specific fuel composition. Y_k is the mass fraction of k^{th} species, superscript *u* denotes unburnt reactant before the flame, and superscript *eq* indicates ideally post-flame chemical equilibrium condition.

This study applies FGM to solve the adiabatic 1-D premixed flamelet in progress variable space, thus two transport equations are required to transform the species mass fraction Y_k and temperature *T* from physical space to progress variable space[30][34]:

$$\boldsymbol{\rho \frac{\partial Y_k}{\partial t} + \frac{\partial Y_k}{\partial c} \dot{\omega}_c = \rho X_c \frac{\partial^2 Y_k}{\partial c^2} + \dot{\omega}_k} \quad (2)$$

$$\boldsymbol{\rho \frac{\partial T}{\partial t} + \frac{\partial T}{\partial c} \dot{\omega}_c = \rho X_c \frac{\partial^2 T}{\partial c^2} - \frac{1}{C_p} \sum_{k=1}^{k=n} h_k \dot{\omega}_k + \frac{\rho X_c}{C_p} \left(\frac{\partial C_p}{\partial c} + \sum_{k=1}^{k=n} C_{p,k} \frac{\partial Y_k}{\partial c} \right) \frac{\partial T}{\partial c}} \quad (3)$$

Where ρ denotes density, *t* is time, $\dot{\omega}_k$, h_k and $C_{p,k}$ are the reaction rate, total enthalpy and specific heat of k^{th} species respectively. $\dot{\omega}_c$ is the rate of progress variable *c*. X_c is the scalar dissipation rate, and it is defined as [30][34]:

$$X_c = \frac{\lambda}{\rho C_p} |\nabla c|^2 \quad (4)$$

Where λ is the thermal conductivity. Thus, X_c is a function of *c*, i.e $X_c(c)$ and is usually modelled by:

$$X_c(c) = X_{max} \exp\left(-2(erfc^{-1}(2c))^2\right) \quad (5)$$

Where $erfc^{-1}$ denotes the inverse complementary error function. X_{max} is the maximum scalar dissipation rate within the premixed flamelet, but noticeably X_{max} is a function of mixture fraction *f*. Thus scalar dissipation rate X_c is exactly a function of both progress variable *c* and mixture fraction *f*, i.e $X_c(c,f)$. Therefore the scaler dissipation rate $X_c(c,f)$ at certain mixture fraction is estimated by [30][34]:

$$X_c(f,c) = X_{max}^{sto} \exp\left(-2\left(erfc^{-1}\left(\frac{f}{f_{sto}}\right)\right)^2\right) exp\left(-2\left(erfc^{-1}(2c)\right)^2\right) \quad (6)$$

Where the X_{max}^{sto} denotes the maximum scaler dissipation rate under the stoichiometric mixture fraction, with a default value of $1000 s^{-1}$, however requiring modification based on fuel composition and operating conditions[30][34]. As the hydrogen content is increased, this value is increased allowing the successful generation of the flamelet table.

However, it is acknowledged that FGM has some limitations in predicting the co-firing of CH_4/H_2 blends, mainly due to two assumptions [28][35]: unity Lewis number and constant turbulent Schmidt number. These assumptions affect the accuracy in predicting species transport and fuel/air mixing process. The assumed unity Lewis number reduces in validity as hydrogen content in the fuel blend increases. It goes from rough unity for pure methane to 0.6 for hydrogen[28][35]. Assuming constant turbulent Schmidt number Sc_t throughout the whole flow zone is not necessarily true as the parameter is a function of local turbulence level. Instead of being constant, the parameter will vary among different flow zones [36]-[37]. Similar work of the authors [38] for this conference presents the use of the Eddy-Dissipation Concept (EDC), which shows superior prediction capability than the FGM model for the technically premixed PRECCINSTA burner. Rather than pre-processing it as in the FGM, the EDC combines detailed chemistry and turbulence to estimate the local mixture transport properties. Yet, such an approach costs more computational time, about 20 times than the FGM, to resolve the transport equations of each species, particularly in such a complex and detailed practical burner configuration considered in this study.

Regarding the NOx emissions, three major pathways are generally considered, including thermal NOx, prompt NOx and intermediate N_2O. Where thermal NOx is a result of the oxidation of nitrogen, showing a strong function with temperature; prompt NOx is a result of the reactions between CH radical and N_2, usually produced near the flame front surface, showing a function with carbon atoms concentration; intermediate N_2O is produced by combining N_2 with atomic oxygen *O*, which prefers high pressure [9][30]. The present study evaluates the NOx of the combustor based on the NOx reaction mechanisms included in GRI-3.0 [25], such as:

$$O + N_2 \rightleftharpoons N + NO \quad (7)$$

$$CH + N_2 \rightleftharpoons HCN + N \quad (8)$$

$$N_2 + O + M \rightleftarrows N_2O + M \quad (9)$$

$$N_2O + O \rightleftarrows 2NO \quad (10)$$

Where **Equation (7)** dominates the thermal NOx reaction; **Equation (8)** controls the prompt NOx; and **Equations (9)-(10)**

determine the NOx via N_2O [9][30]. It should be noted that the present preliminary RANS study could only qualitatively evaluate NO_x emission with different hydrogen blends.

Table 1 the baseline operating parameters used with pure methane, for which the pressure P, temperature T_{air}, air flow $\dot{m}_{air}$, fuel temperature T_{fuel}, and energy input P_{th} are typical of full load conditions of a heavy-duty gas turbine. The air mass flow shown here is 1/4 the total air mass flow, given that only one-quarter of the can was considered.

Table 1. Fixed Operating Parameters

P[bar]	T_{air}[K]	$\dot{m}_{air}$[kg/s]	T_{fuel}[K]	P_{th} [kW]
15.2	692	5.869	413	8628

Figure 4 shows the work of the authors reported in Wiranegara et al. [19] and presents a comparison with the experimental work of Ruan et al. [32] on pure methane. The comparison shows radial profiles of temperature and CO_2 fractions at different planes, indicating that the flame is stabilized at the CRZ, and the chamber wall is surrounded by film cooling flow. The data presented in **Figure 4** were normalized by referring to the maximum value in planes A (330mm) and B (420mm) downstream of the main nozzle exit. This shows that the model could capture major flame characteristics with pure methane as the baseline, although with some discrepancies from experimental results.

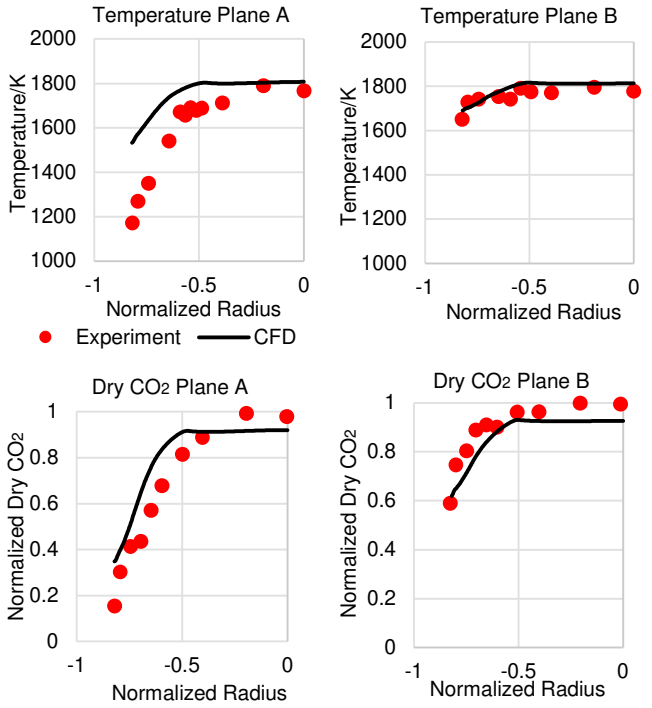

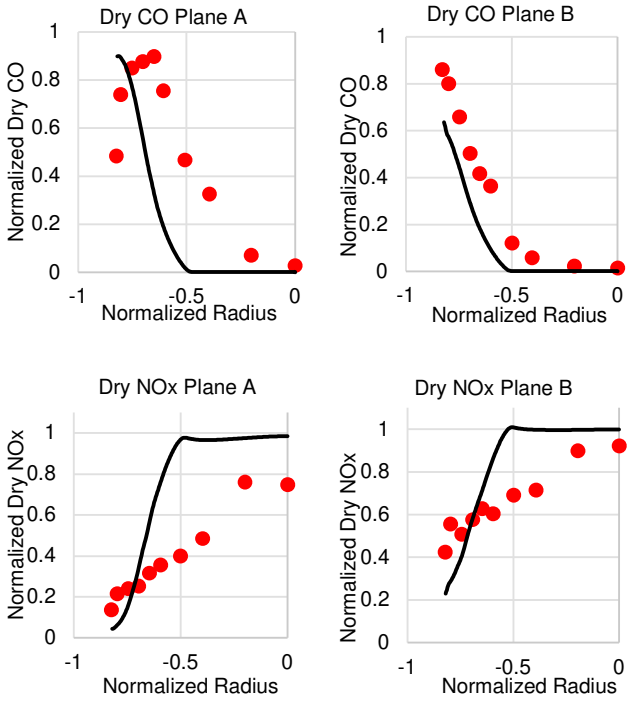

Figure 4. The radial flame temperature and dry mole fraction of CO_2, CO and NOx on two vertical planes [19]

For the investigation on the fuel blends, the same energy input was used as in the baseline (methane-only) case as shown in **Table 1**. Hydrogen concentrations up to 90vol% have been considered. **Table 2** shows the mass fraction of hydrogen, total fuel mixture mass flow and the global equivalence ratio. Also, the total mass flow of the fuel mixture reduces with increased hydrogen content, as hydrogen has a larger specific energy (MJ/kg). The global equivalence ratio also decreases.

Table 2. Operating conditions with H_2/CH_4 blends

$H_2 vol\%$	$H_2 mass\%$	$\dot{m}_{fuel}\ kg/s$	Φ_{global}
0	0.00	0.1719	0.5025
10	1.37	0.1686	0.4998
20	3.03	0.1649	0.4967
30	5.08	0.1605	0.4930
40	7.70	0.1552	0.4886
50	11.11	0.1488	0.4833
60	15.79	0.1408	0.4766
70	22.58	0.1306	0.4681
80	33.33	0.1172	0.4570
90	52.94	0.0987	0.4416

3. PRELIMINARY ANALYSIS OF THE COMBUSTOR

This section covers the fundamental flame characteristics of the baseline case and qualitatively compared it with the simulation of a similar burner, in this case, the Mitsubishi M501G1 burner. Flow pattern and flame shape across the

combustor and the fuel distribution at the main nozzle exit are considered.

Figure 5a shows the basic flow pattern of this CFD model at the main mid-plane, as marked in **Figure 2a**, coloured by flame temperature. The axial swirler in the pilot nozzle contributes to creating a centre recirculation zone (CRZ) to stabilize the pilot diffusion flame. In turn, the flame thus provides some heat and reactants to stabilize the main premixed flame, which can be observed surrounding the pilot flame. The mechanism helps to extend the flammability of the burner under lean conditions, thus providing more flexibility in fuel scheduling. **Figure 5b** shows published results of a similar burner from Mitsubishi M501G1 gas turbine [22]. Despite not being 100% identical, due to a difference in the main nozzle configuration (indicated by the red dashed line), a similar flow pattern and flame shape can be observed between the first two figures. **Figure 5c** shows the flow field from the pilot mid-plane for comparison with the main nozzle mid-plane. Despite the differences in the two configurations, the overall flow pattern is very similar.

Another qualitative comparison was also made for the fuel distribution (normalized equivalence ratio) at the main nozzle exit predicted by our model with PLIF measurements on the Mitsubishi burner[22], displayed in **Figure 6**. Similar fuel distribution can be seen from the comparison, indicating a good prediction of the present model in capturing prominent features of the fuel/air mixing in the main nozzle.

The quantitative and qualitative comparisons presented in **Figure 4, Figure 5,** and **Figure 6**Figure 6 show that the present model can capture the main flow, mixing and combustion characteristics of this type of combustor, hence allowing it to be used for further investigations into the impact of changing conditions.

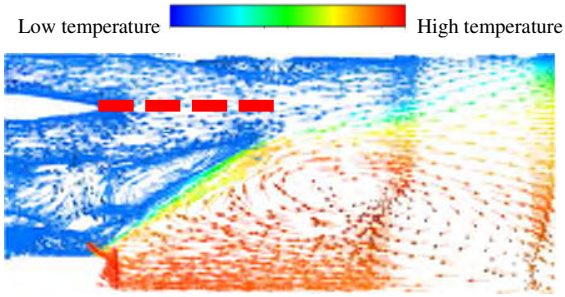

(a) The present study: main mid-plane flow pattern coloured by temperature

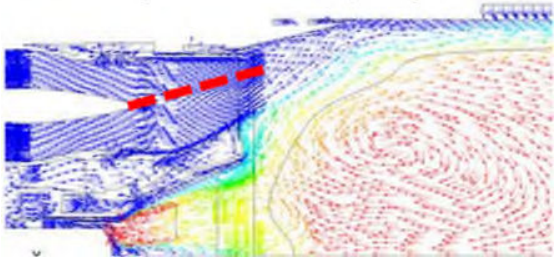

(b) MHI M501G1 burner main mid-plane flow field coloured by temperature [22]

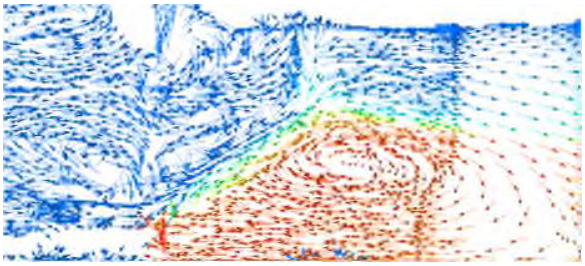

(c) Present study pilot mid-plane flow field coloured by temperature

Figure 5. Velocity vectors of the present study and Ref [22]

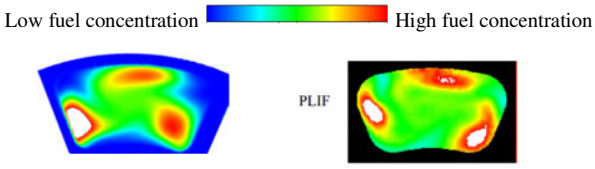

(a) Current CFD model

(b) PLIF-measured [22]

Figure 6. Fuel distribution at the main nozzle exit of the present study and Ref [22]

A temperature contour plot at the main mid-plane across the combustor with pure methane is shown in **Figure 7**. It shows that the pilot diffusion flame is stabilized in the CRZ, producing a relatively high temperature at the pilot nozzle exit. This is due to the split of air flows to the pilot nozzle and main nozzle (which are simply determined by the design of the burner) and the defined pilot/main fuel split. As a result, the pilot region has a higher local equivalence ratio than the main region. The main fuel is premixed with air in the mixing tube before entering the combustion zone, thus producing a relatively uniform fuel distribution and uniform flame temperature, thus avoiding the formation of hotspots whilst also controlling NOx emissions.

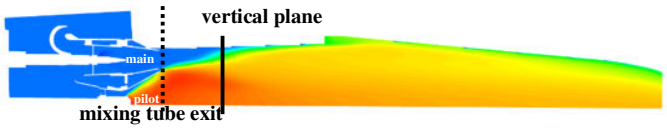

Figure 7. The contour of temperature at the main mid-plane

4. ANALYSIS OF HYDROGEN AND METHANE CO-FIRING

In this section, the combustion characteristics of co-firing hydrogen and methane are investigated using contour plots of several parameters, namely temperature, OH mass fraction, and equivalence ratio. These are presented at three planes, including mid-planes of the main and pilot burner respectively, and a downstream vertical plane. **Figure 8** and **Figure 9** show the temperature contours of 0% to 80vol% hydrogen at the mid-planes of the main and pilot respectively. Results for 90vol% hydrogen are not included in these plots as a flashback is seen. The results will be discussed separately.

In **Figure 8** [**a – e**], for up to 40vol% hydrogen, the change in temperature field is not significant, with a gradual decrease in pilot flame length, due to enhanced fuel reactivity. For higher concentrations of hydrogen from 50vol% to 70vol% **[f – h]**, a larger impact on the flame pattern is seen. The change in the flame characteristic can be attributed to the early ignition of the fuel, emitted from the main nozzle. This is confirmed by the corresponding OH contours shown subsequently. Due to its interaction with the pilot flame region, the combustion happens closer to the main mixing tube outlet, as shown in **Figure 9 [f – h]** on the temperature contours at the pilot mid-plane.

Figure 9 shows the temperature field on the pilot mid-plane showing the fuel and flame of the pilot. The high temperatures can be observed in the area close to the main nozzle outlet for hydrogen concentrations from 50vol% to 70vol%, as marked in **Figure 9 [f – h]**. Yet, this is not seen on the main nozzle mid-plane in **Figure 8 [f – h]**. The region is also not seen at lower hydrogen concentrations in **Figure 9 [a – e]** and at 80vol% in **Figure 9 [i].** This is due to the impact of hydrogen concentration on the momentum of the fuel jets. The changed momentum of the fuel jet impacts the fuel placement. The phenomenon can be explained using Holdeman's correlation [39], which shows a progressive increase in jet penetration with more hydrogen concentrations, but then reduces at higher volumes. Thus, the fuel distribution shows a non-linear function of hydrogen content, and 80vol% does not necessarily follow the behaviours of 60vol% and 70vol%.

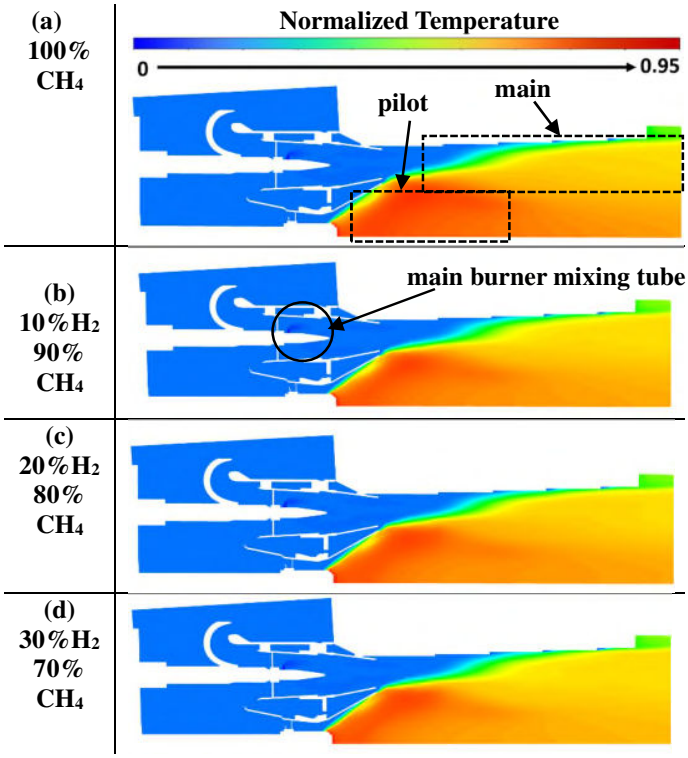

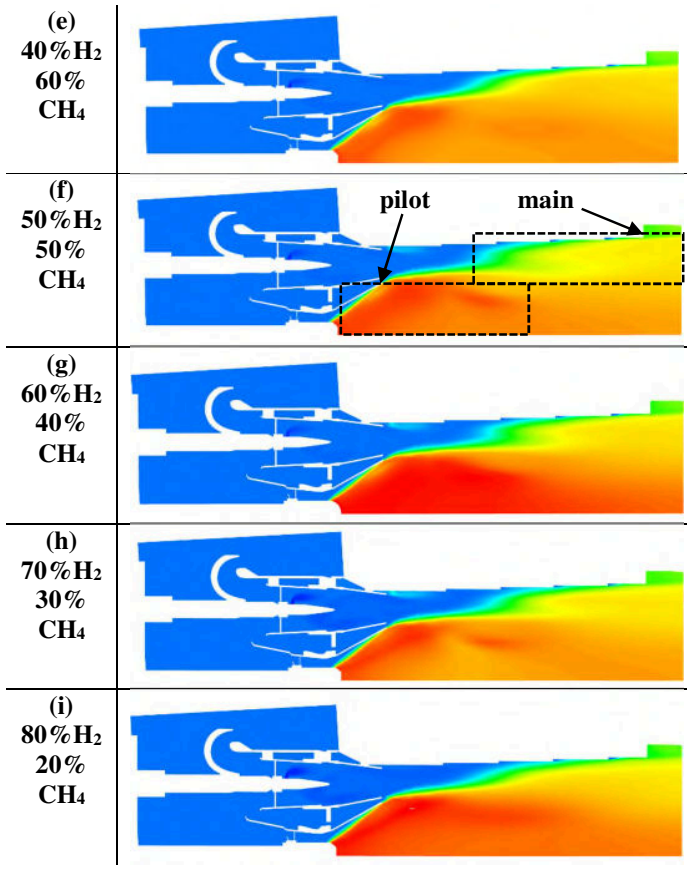

Figure 8. Contours of temperature at main mid-plane for different H_2/CH_4 blends

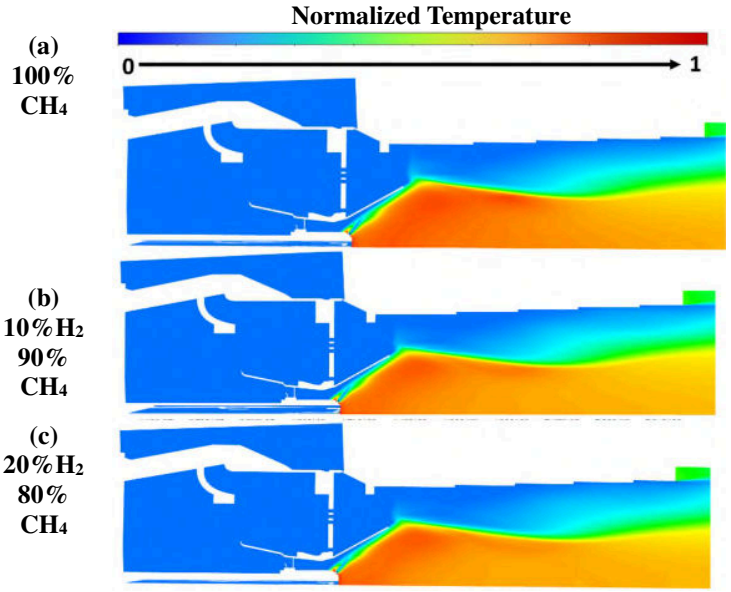

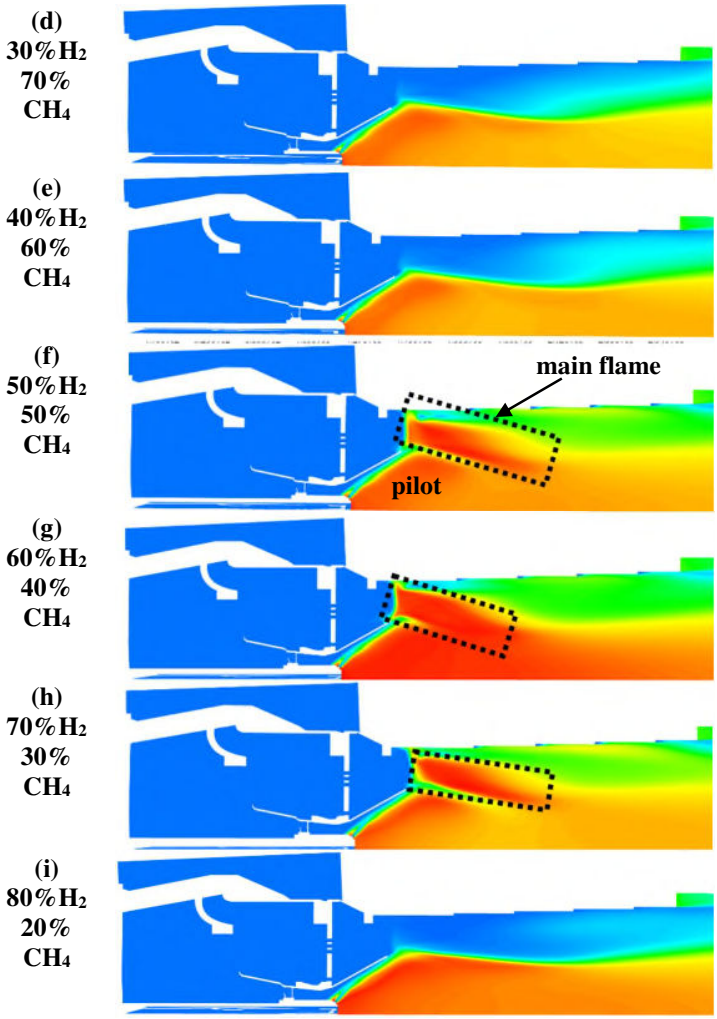

Figure 9. Contours of temperature at pilot mid-plane for different H_2/CH_4 blends

At 90vol% hydrogen, a flashback occurred. This is seen in **Figure 10** (upper image) where high temperatures are seen, particularly along the main mixing tube walls, indicating boundary layer flashback. The flame then propagates back to the fuel nozzle forming a diffusion flame on the fuel jet. This occurs because of the significantly enhanced fuel reactivity and the presence of a flammable mixture in the low velocity region close to the main mixing tube walls. It should be noted that this figure is presented on a different temperature scale than that in **Figure 8**, due to higher maximum temperatures than in the cases of up to 80vol% hydrogen.

Figure 11 shows the OH field which indicates the location and intensity of heat release [2]. It shows the mass fraction of OH on the main mid-plane from 0 to 90vol% hydrogen. High-hydrogen flames produced much higher OH concentrations than the low ones. To allow clear visualization of the flames, three different normalized concentration scales were used to present the OH fields in three groups: 0 to 40vol% H_2 **[a – e]**, 50 to 70vol%H_2 **[f – h]** and 80 to 90lvol%H_2 **[i – j]. Figure 11 [a – e]** shows that from 0 to 40vol% H_2, the flame length indicated by OH decreases as the hydrogen content increases, as expected, due to enhanced fuel reactivity. At higher hydrogen concentrations (from 50 to 70vol%), the expected progressive decrease in flame length did not occur. However, significantly different flame shapes are seen. This is attributed to the early ignition of the fuel, emitted from the main nozzle, due to an interaction with the pilot flame region, leading to combustion closer to the mixing tube outlet, as shown previously in **Figure 9 [f – h]**, marked by the black dashed-rectangles. This early combustion phenomenon is also seen on the vertical plane in **Figure 12 [f – h]**, marked by the black dashed rectangles, where the location of this vertical plane is shown in **Figure 7**. As previously discussed, this is due to the impact of hydrogen addition on fuel placement.

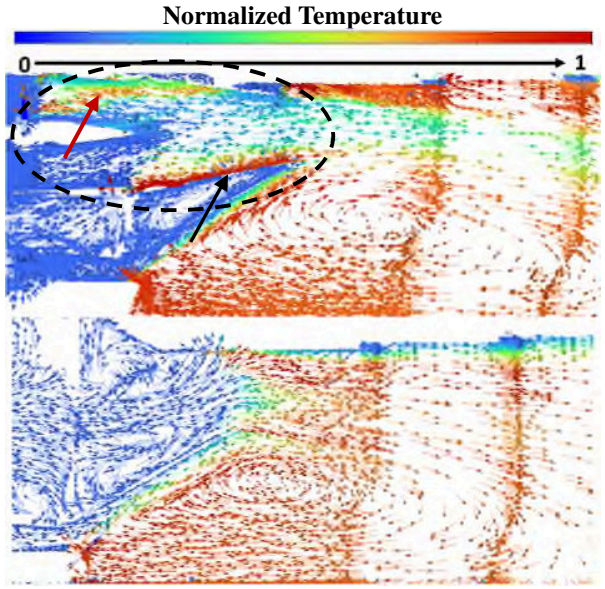

Figure 10. Flow vector at main (top) and pilot (bottom) mid-planes for 90vol%H_2, coloured by temperature

Figure 13 shows that fuel emitted from the main nozzle is increasingly encroaching on the pilot mid-plane and for hydrogen concentrations of 50 to 70vol% hydrogen. Local high equivalence ratios can be observed occurring close to the mixing tube outlet. This results in a significant change in flame pattern from 50vol% to 70vol% as shown previously in **Figure 9 [f – h]**. The concentration peaks at 60vol% hydrogen and then reduce as predicted by the Holdeman correlation. At 80vol% hydrogen (**Figure 13 [i]**), the concentration is sufficiently low to prevent interaction with the pilot flame zone.

The impact of hydrogen addition is also seen in the axial temperature profile of **Figure 14,** which shows the mass-weighted mean temperature for a series of axial planes and is plotted against the axial location, from the burner exit to the combustor outlet. Due to early combustion, the normalized temperature for blend cases of 50 to 70vol% hydrogen produced the quickest temperature rise along the axial distance. This is delayed in the 80vol% hydrogen case, as a result of changed fuel

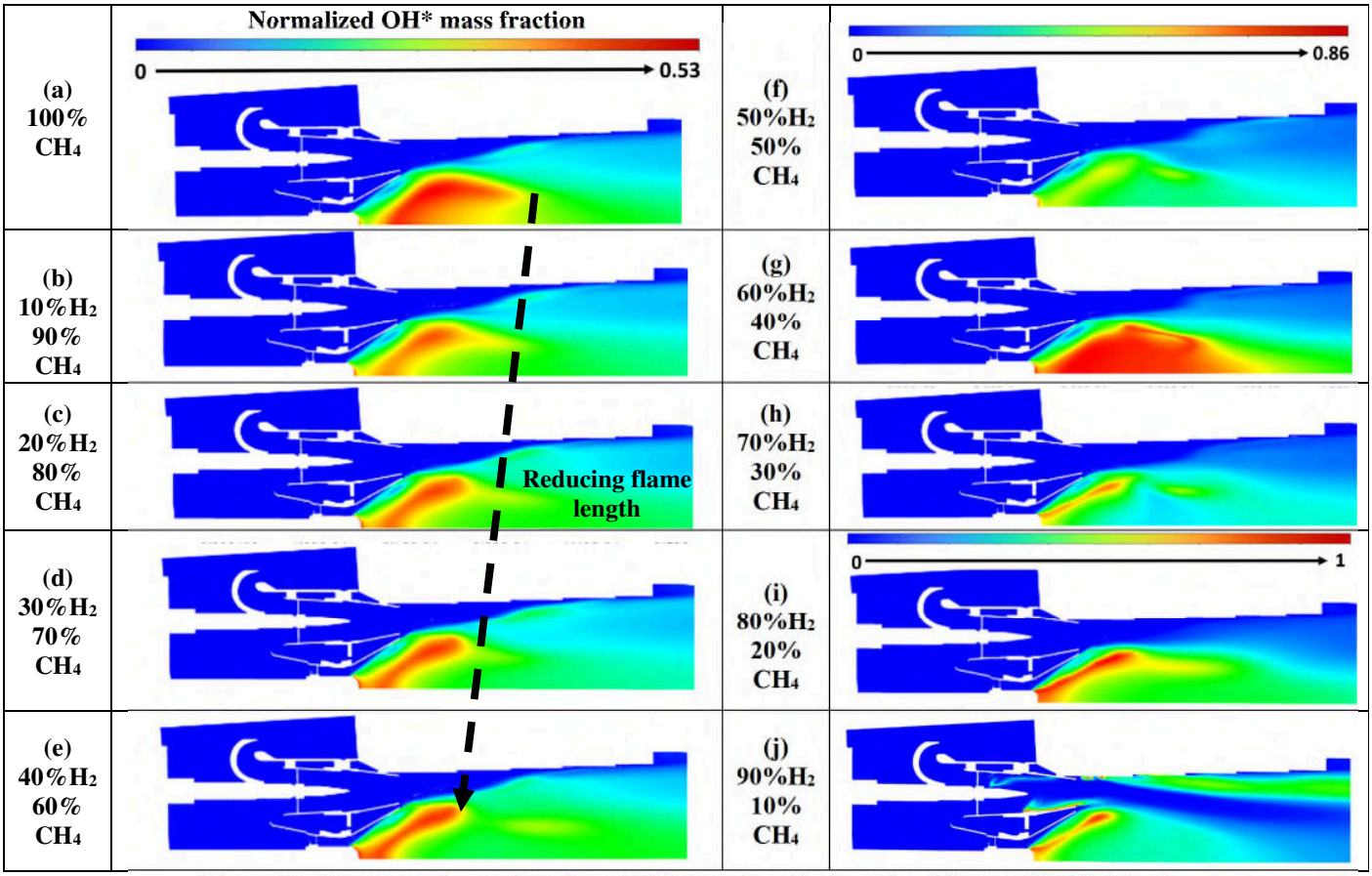

Figure 11. Contours of mass fraction of OH at main mid-plane for different CH_4/H_2 blend

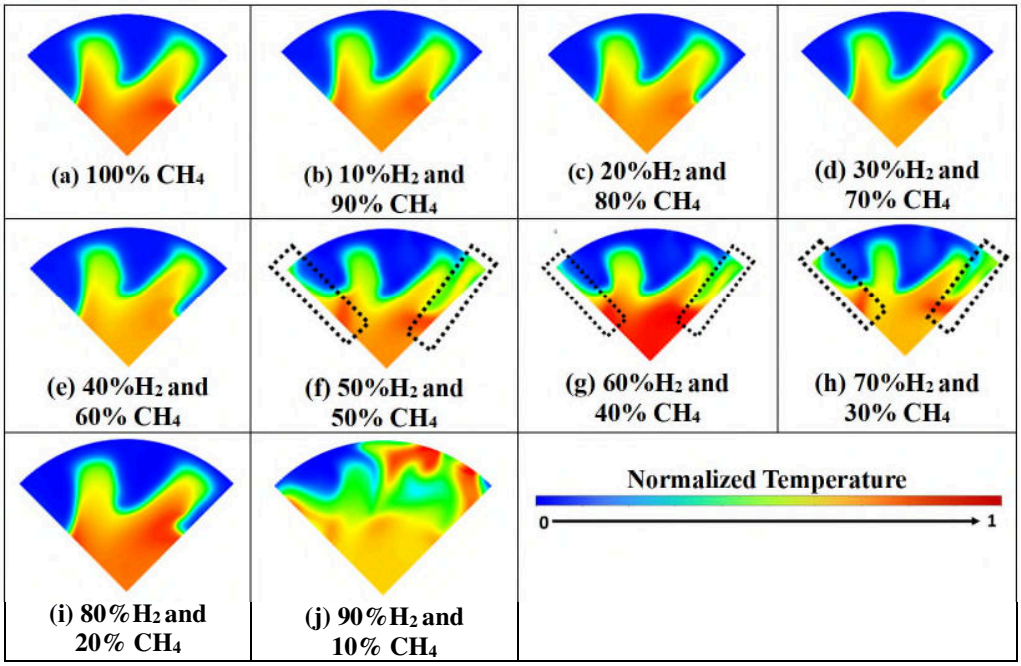

Figure 12. Contours of temperature at the downstream vertical plane for different H_2/CH_4 blends

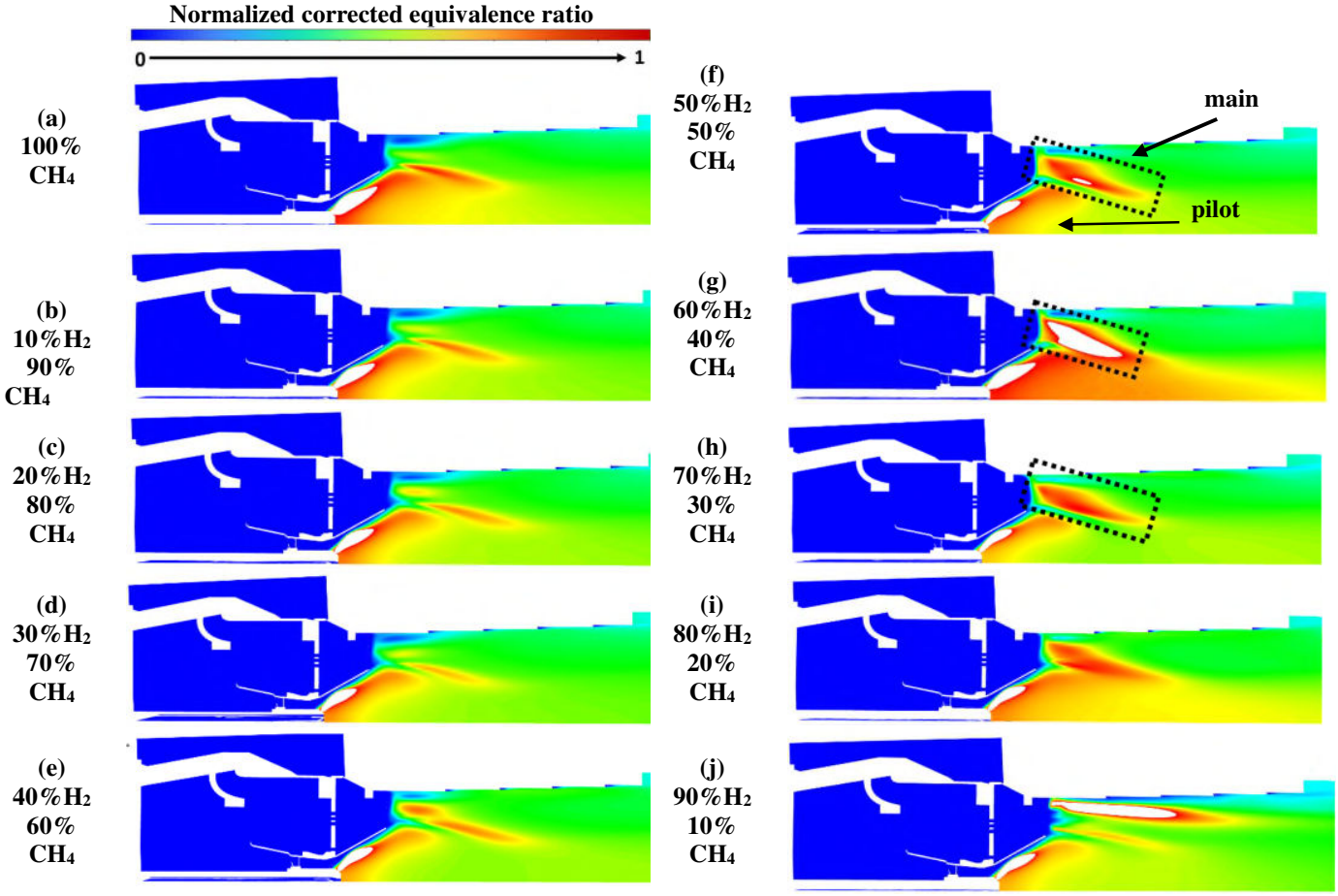

Figure 13. Contours of corrected equivalence ratio at pilot mid-plane for different H_2/CH_4 blends

distribution (due to more hydrogen addition, presented in **Figure 13 [i]**) which didn't result in the early combustion close to the mixing tube outlet, as shown in **Figure 9 [i]**.

Figure 15 shows the combustor outlet temperature for the different blends, which is seen to be relatively stable before a drop at 70vol% and 80vol% hydrogen. The drops are possibly attributed to the influence of varied fuel composition on the dissociation level of CO_2 and H_2O under high temperatures, which impacts the combustor outlet temperature. The figure also shows that there is a progressive increase in the specific heat capacity, Cp, with an increase in hydrogen content that is due to more water vapour produced during the combustion. This is related to the corresponding drop in the calculated non-dissociated adiabatic flame temperature when hydrogen content is increased. Also, the combustor outlet temperature is observed to be lower than the calculated non-dissociated adiabatic flame temperature, due to the dissociation of CO_2 and H_2O under high-temperature conditions. The maximum difference is 25 °C seen at 80vol% hydrogen case.

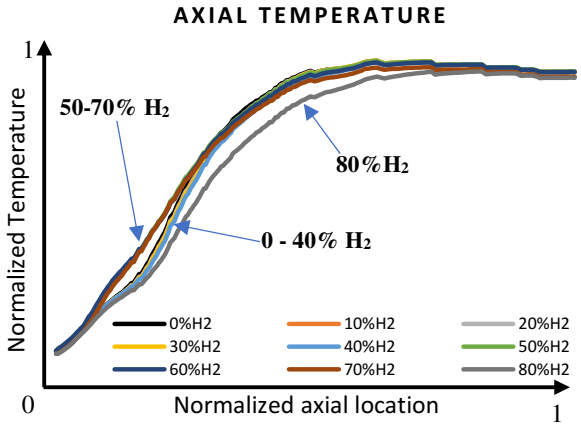

Figure 14. Mass-weighted temperature against the axial location for different H_2/CH_4 blends

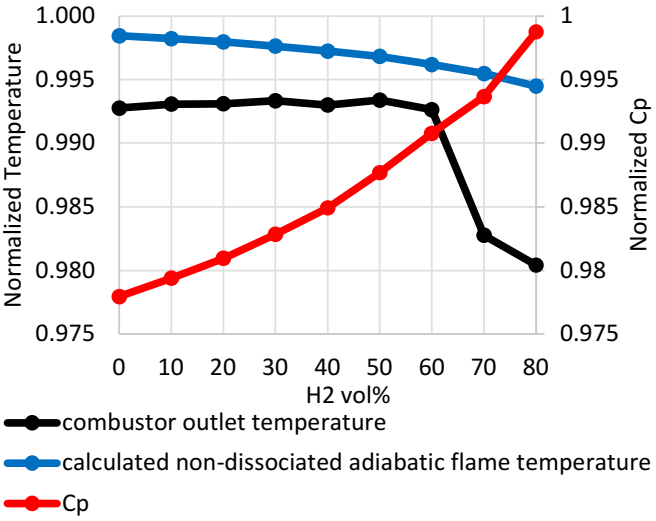

Figure 15 Normalized temperature (combustor outlet and calculated non-dissociated flame temperature) and specific heat for different H_2/CH_4 blends

Figure16 shows the NO_X and unmixedness for the range of blends of hydrogen and methane. The unmixedness indicates the mixing quality of fuel and air, where lower unmixedness indicates better mixing quality. Wiranegara et al. [19] mathematical definition of unmixedness was used in this study to show the relationship between NO_X production and unmixedness. From the figure, it can be observed that the profile of unmixedness shows a non-linear function with hydrogen content, as the fuel distribution is impacted by the hydrogen content non-linearly. This is consistent with the observations presented earlier in **Figure 13**. The NO_X emissions are seen to increase as the concentration of hydrogen increases to 60vol%. Nevertheless, there is a drop at 70vol% hydrogen which is again followed by a rise at 80vol% hydrogen. The drop is likely to be partly influenced by the unmixedness which is particularly low in this case, as shown in the figure. This is also related to the lower outlet temperature observed in the 70vol% and 80vol% hydrogen cases presented in **Figure 15.** It is important to note that two ways of reporting NO_x emissions are presented. These are the conventional manner in parts per million by volume (ppmv) corrected to 15%O_2 and dry conditions and a mass per fuel energy input basis (g/J). Compared to natural gas or methane combustion, hydrogen-enriched natural gas flames produce more water vapour and consume less oxygen. This results in hydrogen combustion having a higher NOx when presented conventionally than a natural gas flame that produces the same absolute mass of NOx[40]. Reporting on a mass per fuel energy input basis provides a fairer comparison of the absolute NOx emissions to the atmosphere [40]-[41].

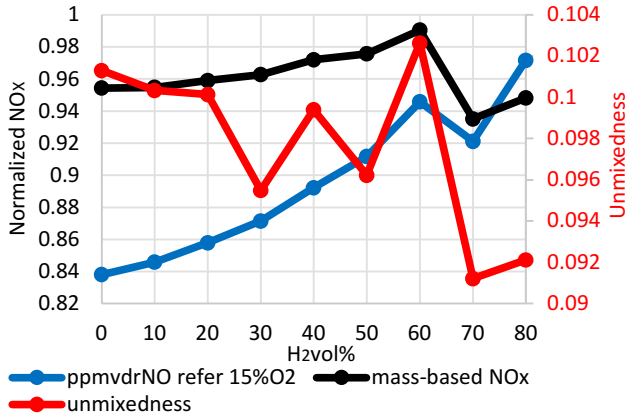

Figure16. NO_X (volume concentration and mass-based) and unmixedness for different H_2/CH_4 blends

7. CONCLUSIONS

In summary, the present study has shown the impact of increasing hydrogen content (0 to 90vol%) in methane-hydrogen blends at high combustor operating pressure in a practical gas turbine DLN combustor. The CFD analysis performed at constant energy input in this industry-scale partially premixed burner showed:

- As hydrogen was increased up to 40vol%, the flame length progressively decreased, as shown in the OH results.
- This was not the case for 50 to 70vol% H_2, for which significantly different flame shapes were observed. This was attributed to some fuel emitted from the mixing tube encroaching on the pilot flame region and igniting closer to the mixing tube outlet.
- Flashback occurred at 90vol% H_2, due to significantly enhanced fuel reactivity and the high fuel concentration close to the mixing tube wall.
- As hydrogen concentration increased, the specific heat capacity of the combustion rose due to more water vapour being produced. This in turn caused reductions in the adiabatic flame temperature even though there was constant air flow and constant fuel energy input.
- NO_X emissions were evaluated on both a corrected ppmv basis and a mass basis per unit of fuel energy basis. NO_X emission increased as the hydrogen was increased up to 60vol%. However, a drop in NO_x was observed at 70vol% hydrogen and then an increase at 80vol% hydrogen. This has been linked to the changes in the unmixedness and combustor outlet temperature.
- As hydrogen concentration was increased, NO_x quoted on a corrected ppmv basis showed a larger increase than that quoted on a mass-energy basis due to the impact of hydrogen on the water and oxygen corrections. Hence, absolute NOx production is better represented using the mass-energy approach.
- Finally, it should be noted that as natural gas is more reactive than methane, it is expected that using natural gas is likely to be slightly more pessimistic in the predictions.

REFERENCES

[1] Griffiths, A., and Syred, N., 2010, "Flashback Limits of Premixed H2/CH4 Flames in a Swirl-Stabilized Combustor," *Proceedings of ASME Turbo Expo*, Glasgow, UK, pp. 1–12.

[2] Chterev, I., and Boxx, I., 2021, "Effect of Hydrogen Enrichment on the Dynamics of a Lean Technically Premixed Elevated Pressure Flame," Combust. Flame, **225**, pp. 149–159.

[3] Griebel, P., Boschek, E., and Jansohn, P., 2007, "Lean Blowout Limits and NOx Emissions of Turbulent, Lean Premixed, Hydrogen-Enriched Methane/Air Flames at High Pressure," J. Eng. Gas Turbines Power, **129**(2), pp. 404–410.

[4] Sakhrieh, A., 2019, "The Adiabatic Flame Temperature and Laminar Flame Speed of Methane Premixed Flames at Varying Pressures," Acta Period. Technol., **50**, pp. 220–227.

[5] Brower, M., Petersen, E. L., Metcalfe, W., Curran, H. J., Füri, M., Bourque, G., Aluri, N., and Güthe, F., 2013, "Ignition Delay Time and Laminar Flame Speed Calculations for Natural Gas/Hydrogen Blends at Elevated Pressures," J. Eng. Gas Turbines Power, **135**(2), pp. 1–10.

[6] Ebi, D., and Jansohn, P., 2021, "Boundary Layer Flashback Limits of Hydrogen-Methane-Air Flames in a Generic Swirl Burner at Gas Turbine-Relevant Conditions," J. Eng. Gas Turbines Power, **143**(8), pp. 1–7.

[7] Lin, Y., Daniele, S., Jansohn, P., and Boulouchos, K., 2013, "Turbulent Flame Speed as an Indicator for Flashback Propensity of Hydrogen-Rich Fuel Gases," *Proceedings of ASME Turbo Expo*, San Antonio, Texas, USA, pp. 1–10.

[8] Fiolitakis, A., Luckerath, R., Lammel, O., Schmiz, G., Ax, H., Stohr, M., Arndt, C., and Noll, B., 2018, "Assessment of a Finite-Rate-Chemistry Model for Ansys CFD Using Experimental Data of a Downsized Gas Turbine Combustor," *Proceedings of ASME Turbo Expo*, pp. 1–11.

[9] Glarborg, P., Miller, J. A., Ruscic, B., and Klippenstein, S. J., 2018, "Modeling Nitrogen Chemistry in Combustion," Prog. Energy Combust. Sci., **67**, pp. 31–68.

[10] "Hydrogen Gas Turbine" [Online]. Available: https://etn.global/wp-content/uploads/2020/02/ETN-Hydrogen-Gas-Turbines-report.pdf. [Accessed: 24-Jun-2021].

[11] "Mitsubishi Power | The Hydrogen Gas Turbine, Successfully Fired with a 30% Fuel Mix, Is a Major Step towards a Carbon-Free Society" [Online]. Available: https://power.mhi.com/special/hydrogen/article_1. [Accessed: 11-Nov-2022].

[12] "Siemens' Roadmap to 100% Hydrogen Gas Turbines" [Online]. Available: https://www.powermag.com/siemens-roadmap-to-100-hydrogen-gas-turbines/. [Accessed: 10-Nov-2022].

[13] "SGT-300 | Industrial Gas Turbine | Gas Turbines | Manufacturer | Siemens Energy Global" [Online]. Available: https://www.siemens-energy.com/global/en/offerings/power-generation/gas-turbines/sgt-300.html. [Accessed: 10-Nov-2022].

[14] "SGT-800 | Industrial Gas Turbine | Gas Turbines | Manufacturer | Siemens Energy Global" [Online]. Available: https://www.siemens-energy.com/global/en/offerings/power-generation/gas-turbines/sgt-800.html. [Accessed: 10-Nov-2022].

[15] "SGT-A35 | Aeroderivative Gas Turbine | Gas Turbines | Manufacturer | Siemens Energy Global" [Online]. Available: https://www.siemens-energy.com/global/en/offerings/power-generation/gas-turbines/sgt-a30-a35-rb.html. [Accessed: 10-Nov-2022].

[16] "Hydrogen" [Online]. Available: https://www.ansaldoenergia.com/offering/solutions-for-the-transition/hydrogen. [Accessed: 10-Nov-2022].

[17] "GT36" [Online]. Available: https://www.ansaldoenergia.com/offering/equipment/turbomachinery/gt36. [Accessed: 10-Nov-2022].

[18] Emerson, B., Wu, D., Lieuwen, T., Noble, D., Sheppard, S., and Angello, L., 2020, "Assessment of Current Capabilities and Near-Term Availability of Hydrogen-Fired Gas Turbines Considering a Low-Carbon Future," *Proceedings of the ASME Turbo Expo*, pp. 1–10.

[19] Wiranegara, R. Y., Igie, U., Ghali, P., Zhao, R., Abbott, D., and Hamilton, R., 2022, "Numerical Study of Radiation and Fuel – Air Unmixedness on the Performance of a Dry Low NOx Combustor," ASME Open J. Eng., **1**, pp. 1–13.

[20] Meier, W., Weigand, P., Duan, X. R., and Giezendanner-Thoben, R., 2007, "Detailed Characterization of the Dynamics of Thermoacoustic Pulsations in a Lean Premixed Swirl Flame," Combust. Flame, **150**(1–2), pp. 2–26.

[21] Runyon, J., Marsh, R., Pugh, D., Bowen, P., Giles, A., Morris, S., and Valera-Medina, A., 2017, "Experimental Analysis of Confinement and Swirl Effects on Premixed Ch4-H2 Flame Behavior in a Pressurized Generic Swirl Burner," *Proceedings of the ASME Turbo Expo*, pp. 1–12.

[22] Tanimura, S., Nose, M., Ishizaka, K., Takiguchi, S., and Rodriguez, J., 2008, "Advanced Dry Low Nox Combustor for Mitsubishi G Class Gas Turbines," *Proceedings of the ASME Turbo Expo*, pp. 607–615.

[23] ANSYS Inc., 2021, *FLUENT User's Guide 21 R1*.

[24] Wang, K., Li, F., Zhou, T., and Ao, Y., 2023, "Numerical Study of Combustion and Emission Characteristics for Hydrogen Mixed Fuel in the Methane-Fueled Gas Turbine Combustor," Aerospace, **10**(1).

[25] "GRI-Mech 3.0" [Online]. Available: http://combustion.berkeley.edu/gri-mech. [Accessed: 19-Nov-2021].

[26] Donohoe, N., Heufer, A., Metcalfe, W. K., Curran, H. J., Davis, M. L., Mathieu, O., Plichta, D., Morones, A., Petersen, E. L., and Güthe, F., 2014, "Ignition Delay Times, Laminar Flame Speeds, and Mechanism Validation for Natural Gas/Hydrogen Blends at Elevated Pressures," Combust. Flame, **161**(6), pp. 1432–1443.

[27] Metcalfe, W. K., Burke, S. M., Ahmed, S. S., and Curran, H. J., 2013, "A Hierarchical and Comparative Kinetic Modeling Study of C1 - C2 Hydrocarbon and Oxygenated Fuels," Int. J. Chem. Kinet., **45**(10), pp. 638–675.

[28] Shrivastava, S., Verma, I., Yadav, R., Nakod, P., and Orsino, S., 2021, "Comparison of Performance of Flamelet Generated Manifold Model with That of Finite Rate Combustion Model for Hydrogen Blended Flames," *Proceedings of the ASME Turbo Expo*, pp. 1–13.

[29] Zghal, M., Sun, X., Gauthier, P. Q., and Sethi, V., 2020, "Comparison of Tabulated and Complex Chemistry Turbulent-Chemistry Interaction Models with High Fidelity Large Eddy Simulations on Hydrogen Flames," *Proceedings of the ASME Turbo Expo*, pp. 1–11.

[30] ANSYS Inc., 2021, *Ansys Fluent Theory Guide 21 R1*.

[31] Ottino, G. M., Fancello, A., Falcone, M., Bastiaans, R. J. M., and De Goey, L. P. H., 2016, "Combustion Modeling Including Heat Loss Using Flamelet Generated Manifolds: A Validation Study in OpenFOAM," Flow, Turbul. Combust., **96**(3), pp.

773–800.

[32] Ruan, S., Swaminathan, N., Isono, M., Saitoh, T., and Saitoh, K., 2015, "Simulation of Premixed Combustion with Varying Equivalence Ratio in Gas Turbine Combustor," J. Propuls. Power, **31**(3), pp. 861–871.

[33] Langone, L., Amerighi, M., and Andreini, A., 2022, "Large Eddy Simulations of a Low-Swirl Gaseous Partially Premixed Lifted Flame in Presence of Wall Heat Losses†," Energies, **15**(3).

[34] Nakod, P., Yadav, R., Rajeshirke, P., and Orsino, S., 2014, "A Comparative Computational Fluid Dynamics Study on Flamelet-Generated Manifold and Steady Laminar Flamelet Modeling for Turbulent Flames," J. Eng. Gas Turbines Power, **136**(8), pp. 1–8.

[35] Sun, X., Agarwal, P., Carbonara, F., Abbott, D., Gauthier, P., and Sethi, B., 2020, "Numerical Investigation into the Impact of Injector Geometrical Design Parameters on Hydrogen Micromix Combustion Characteristics," *Proceedings of the ASME Turbo Expo*, pp. 1–11.

[36] He, G., Guo, Y., Hsu, A. T., Brankovic, A., Syed, S., and Liu, N. S., 1999, "The Effect of Schmidt Number on Turbulent Scalar Mixing in a Jet-in-Crossflow," *Proceedings of the ASME Turbo Expo*.

[37] Li, S., Zhang, S., Hou, L., and Ren, Z., 2018, "Analysis of the Mixing and Emission Characteristics in a Model Combustor," *Proceedings of the ASME Turbo Expo*, pp. 1–7.

[38] Zhao, R., Igie, U., and Abbott, D., 2023, "Hydrogen-Enriched Natural Gas Co-Firing: A Comparison of FGM and EDC Models," *Proceedings of the ASME Turbo Expo*.

[39] Holdeman, J. D., 1972, "Correlation for Temperature Profiles in the Plane of Symmetry Downstream of a Jet Injected Normal to a Crossflow," NASA Tech. Note NASA TN D-6966, (September).

[40] Douglas, C. M., Shaw, S. L., Martz, T. D., Steele, R. C., Noble, D. R., Emerson, B. L., and Lieuwen, T. C., 2022, "Pollutant Emissions Reporting and Performance Considerations For Hydrogen–Hydrocarbon Fuels in Gas Turbines," *Proceedings of ASME Turbo Expo*, Rotterdam, The Netherlands.

[41] Breer, B., Rajagopalan, H. P., Godbold, C., Ii, J., Emerson, B., Acharya, V., Sun, W., Lieuwen, T., and Noble, D., 2022, "NOx Production from Hydrogen-Methane Blends," *In Spring Technical Meeting of the Eastern States Section of the Combustion Institute, Orlando, FL, Mar. 6-9*, pp. 149RKF–0019.

Cranfield University

CERES https://dspace.lib.cranfield.ac.uk

School of Aerospace, Transport and Manufacturing (SATM) Staff publications (SATM)

2023-09-28

Co-firing of hydrogen and natural gas in a practical DLN combustor model

Zhao, Rang

American Society of Mechanical Engineers

Zhao R, Igie U, Abbott D, Wiranegara RY. (2023) Co-firing of hydrogen and natural gas in a practical DLN combustor model. In: ASME Turbo Expo 2023: Turbomachinery Technical Conference and Exposition, 26-30 June 2023, Boston, USA. Paper number GT2023-103212 https://doi.org/10.1115/GT2023-103212

Downloaded from Cranfield Library Services E-Repository